Measurement of Energies Controlling Ripening and Annealing on Metal Surfaces

Karina Morgenstern,[1,2,*] Georg Rosenfeld,[1,†] Erik Lægsgaard,[2] Flemming Besenbacher,[2] and George Comsa[1,‡]
[1]*Institut für Grenzflächenforschung und Vakuumphysik, Forschungszentrum Jülich GmbH, D-52425 Jülich, Germany*
[2]*Institute of Physics and Astronomy and Center for Atomic-scale Materials Physics, University of Aarhus, DK-8000 Aarhus C, Denmark*
(Received 9 April 1997)

The successful experimental implementation of a powerful concept for the determination of energies controlling ripening and annealing on surfaces is reported. On a Ag(111) surface, we have prepared and studied the decay of well-defined nanostructures for which an available exact theoretical description can be used. The decay is followed by fast scanning tunneling microscopy at various temperatures to determine the 2D evaporation rate of atoms from island edges and the interlayer mass transport. An activation energy for 2D evaporation of (0.71 ± 0.03) eV and an Ehrlich-Schwoebel barrier of (0.13 ± 0.04) eV are determined. [S0031-9007(97)05037-0]

PACS numbers: 68.55.–a, 68.10.Jy, 68.60.Dv, 82.65.Dp

The control of kinetic parameters in thin metal film growth is of utmost importance for the ability to design novel nanoscale structures. Field ion microscopy (FIM) and scanning tunneling microscopy (STM) have led to an unprecedented insight into the basic atomic processes occurring during metal on metal growth: condensation of atoms on the surface [1], diffusion of single atoms on a crystal plane [2], nucleation of atoms into clusters [3], and diffusion across, along, and towards islands or steps [4–7]. Ripening in thin metal films *after* growth is of equal importance. As many nanoscale surface structures are only metastable, it is important to know on what time scale material rearranges and whether these processes can be used for modifying nanostructures on surfaces. A number of recent studies using STM [8–10] and FIM [2,7,11] have addressed this issue for metal surfaces, and, in particular, FIM has been very successful in quantifying the stability of small two-dimensional clusters.

The great advantage of FIM studies is that this technique allows the study of isolated clusters in a well-defined environment: The cluster investigated is the topmost cluster on a stack of layers forming the FIM tip, and it interacts with its environment only via the descending step surrounding it. This simple geometry, which can be approximated very well by two concentric circles, makes it easy to write down expressions for the mass flow from the cluster to the surrounding step. This advantage was realized and used almost forty years ago in studies on the blunting of field emitter tips [12]. However, one disadvantage of studying the topmost cluster on a stack is that the mass flow involves diffusion over a *descending* step. As in many cases, step-down diffusion requires an additional barrier as compared to terrace diffusion (the so-called Ehrlich-Schwoebel barrier [13]); the activation barrier measured in such an experiment is, in general, different from that controlling cluster or island decay in an ensemble of islands, i.e., when the mass flow takes place between *ascending* step edges. On the other hand, the theoretical description of mass flow between ascending island edges in such an ensemble is more difficult. The classical theoretical formalism developed for this case [14–16] does make use of the simple geometry of two concentric circles but the assignment of a boundary condition at the outer circle and the exact location of this (fictitious) outer boundary are based on questionable assumptions.

In view of this dilemma, the best approach for measuring mass transport between ascending island edges in a well-defined way would be to prepare and study a morphology which exactly corresponds to the simple geometry (cf. Fig. 1): a single island surrounded by an *ascending* step edge, i.e., an adatom island placed into a large vacancy island of monoatomic depth. We proposed to perform such experiments in a recent paper on island decay [10], and the power of this approach was also realized by McLean *et al.*, who worked out in detail the extension of the classical theoretical description to the special morphology of an adatom island inside a vacancy island [17]. Moreover, they studied this case in Monte Carlo simulations. In the present paper, we report on the first successful experimental implementation of this concept. In an extensive study on a Ag(111) surface, we show that

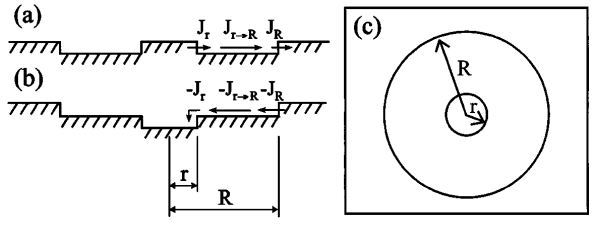

FIG. 1. Schematic view of theoretically modeled geometry with diffusion fluxes: (a) adatom island and (b) vacancy island, both surrounded by an ascending step; (c) top view of (a) and (b).

 0031-9007/98/80(3)/556(4)$15.00

single adatom islands in vacancy islands (cf. Figs. 1 and 2) can indeed be routinely prepared. We study their decay as a function of temperature and are able to determine an activation energy for atom detachment from steps of (0.71 ± 0.03) eV. Moreover, the line tension of two-dimensional islands is estimated to (0.75 ± 0.15) eV/nm. We also study a second generic morphology: vacancy islands inside of vacancy islands (cf. Figs. 1 and 2). The filling of the inner vacancy islands is hindered by the Ehrlich-Schwoebel barrier as observed previously [10] and, hence, a comparison of the filling rate of vacancy islands to the decay rate of adatom islands can be used to estimate the magnitude of the step edge barrier as noted by Ichimiya *et al.* [18]. From our measurements on the Ag(111) surface reported here, we are able to determine an Ehrlich-Schwoebel barrier of (0.13 ± 0.04) eV.

The experiments have been performed in a UHV chamber (base pressure 5×10^{-11} mbar) on a Ag(111) single crystal surface. The model nanostructures are created as follows. On the well prepared clean surface, large vacancy islands are created by removing 0.3 to 0.5 monolayers (ML) by 1 keV Ne^+ sputtering at 373 K, followed by slow cooling to 330 K at a rate of 0.5 K/min. This results in monatomic high vacancy islands of equilibrium shape and diameters between 40 and 300 nm. To place a smaller vacancy island into one of these larger ones, the surface is sputtered briefly (2 to 5 s) at room temperature. Hereby, small monatomic vacancy islands are created within the larger vacancy islands [Fig. 2(b), at 0 s], a few of them concentrically. To place an adatom island within a large vacancy island is more demanding due to the low density of nuclei of Ag/Ag(111). Usually, all adatoms deposited into one of the vacancy islands attach to the island boundary. To force nucleation of an adatom island within a vacancy island, the surface is exposed to a sputter pulse at temperatures between 200 and 250 K to provide nucleation centers prior to Ag deposition. Figure 2(a) (at $t = 0$ s) shows the morphology after a 1 keV Ne^+ pulse and 0.2 ML Ag deposited at 250 K. The substrate temperature is subsequently adjusted to the value at which the experiments are performed. The decay of adatom and vacancy islands has been studied at temperatures between 240 and 310 K, and between 280 and 360 K, respectively.

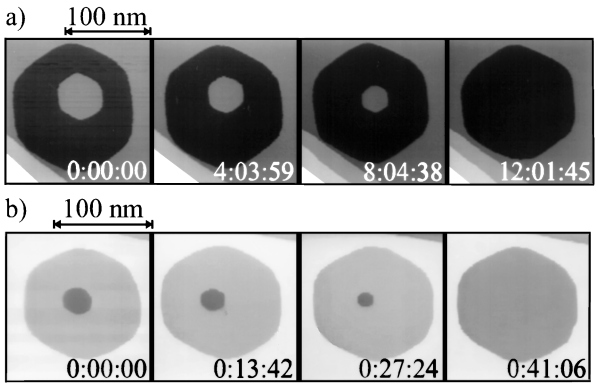

FIG. 2. STM images of decaying islands of monatomic height on Ag(111): (a) adatom island at 300 K, $R = 73$ nm, $U_t = -1.91$ V, $I_t = 0.09$ nA; (b) vacancy island at 360 K, $R = 51$ nm, $U_t = -2$ V, $I_t = 0.1$ nA.

The island decay is monitored by scanning the surface repeatedly with a variable temperature STM of the Rasterscope type [19]. Images of 200 nm $\times$ 200 nm with a resolution of 128 pixels $\times$ 128 pixels are recorded at time intervals of down to 10 s. The STM is very stable with a cylindrical drift compensated design. In addition, we have compensated for the remaining thermal drift using an active tracking technique, which allows us to follow the time evolution of a given structure for more than 50 hours. This is done by defining a template over a prominent structure in an image. For each image, the cross correlation between the template and the actual image is maximized by sliding the template over the image. Position correction is applied to the scanner tube to keep the prominent structure at a constant position in the image. The achieved stability depends on the stability of the structure, but is often ± 1 pixel even over extended periods (days). However, for long-time measurements at temperatures other than room temperature, a slow temperature drift towards room temperature cannot be avoided. This drift is accounted for in the analysis (see below). Figure 2 shows snapshots from two STM movies illustrating the decay of adatom and vacancy islands. Typical tunneling parameters used for the STM imaging are $I_t = 0.1$ nA and $V_t = -2$ V. We established that, under these conditions, there is no tip influence on the results. First, a direct influence on thermally stable structures at temperatures of 180 K was observed only for tunneling resistances at least a factor of one hundred lower than used in the experiments here. Second, we changed the interaction time between tip and investigated object as described earlier [20], and found no effect. In addition, we checked that islands not scanned decay at the same rate as those scanned continuously.

From the STM movies, we determine the island area $A(t)$ as a function of time. Examples for both adatom and vacancy islands are shown in Fig. 3. Obviously, adatom and vacancy islands decay differently, both quantitatively and qualitatively. The decay rate of adatom islands increases with decreasing island size [negative curvature of $A(t)$]. On the contrary, the decay rate of the vacancy island is almost constant resulting in a linear decrease of $A(t)$. Deviations from this apparent linearity are found only when the islands are very small. The fundamental difference reflects the change in the kinetics caused by the Ehrlich-Schwoebel barrier for the vacancy island decay. The data are analyzed using the theory of Ostwald ripening [14–16] including extensions by McLean *et al.* [17]. The model follows a continuum approach and, hence, is expected to break down for very small clusters. However, this would introduce a systematic error only

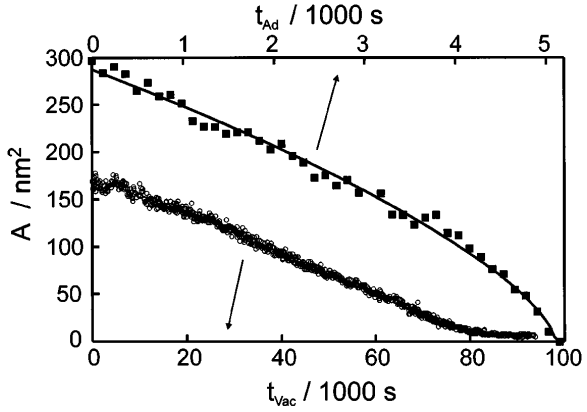

FIG. 3. Area versus time plot at 300 K. Open circles: vacancy island decay (bottom axis); solid squares: adatom island decay (top axis); the solid line represents the best fit of the numerical integration of Eq. (3).

for the line tension which is estimated from the shape of decay curves in the small-size regime (see below), but for which the error is large anyhow. Below, we repeat the main ingredients of the model, starting with adatom islands.

The net flux of particles away from the island, J, is calculated from the three flux contributions indicated in Fig. 1: the (net) detachment flux of adatoms from the inner edge J_r, the (net) diffusion flux over the terrace $J_{r\to R}$, and finally the (net) attachment flux of adatoms to the outer edge J_R. The net flux of atoms from or to an island of radius $\tilde{r}$ is given by [15]

$$J_{\tilde{r}} = \frac{2\pi\tilde{r}D}{a}[\rho_{\mathrm{eq}}(\tilde{r}) - \rho(\tilde{r})], \tag{1}$$

where a is the lattice constant and D is the adatom diffusion constant. $\rho_{\mathrm{eq}}(\tilde{r})$ denotes the equilibrium adatom density in front of a step of curvature $1/\tilde{r}$ as given by the Gibbs-Thomson relation: $\rho_{\mathrm{eq}}(\tilde{r}) = \rho_\infty \exp(\gamma/kTn\tilde{r})$, with the line tension γ and the adatom density in front of a straight step ρ_∞. Finally, $\rho(\tilde{r})$ is the actual adatom density in front of the island edge. Equation (1) describes the net fluxes both at the inner (J_r) and the outer boundary (J_R) [17]. However, at the outer boundary the curvature is negative and, thus, also, the exponent in the Gibbs-Thomson relation is negative. The steady state diffusion flux between the two concentric edges is given by [14]

$$J_{r\to R} = \frac{2\pi D}{\ln(R/r)}[\rho(r) - \rho(R)]. \tag{2}$$

Mass conservation and equality of net fluxes at steady state yields $J = J_r = J_{r\to R} = J_R$, leading to a differential equation for the island radius [15–17]:

$$\frac{d(\pi r^2)}{dt} = -\beta\left[\frac{a}{r} + \ln(R/r) + \frac{a}{R}\right]^{-1} \times \left[\exp\left(\frac{\gamma}{kTnr}\right) - \exp\left(-\frac{\gamma}{kTnR}\right)\right], \tag{3}$$

with the temperature-dependent factor $\beta = 2\pi D\rho_\infty/n$, where n is the atomic density. The temperature dependence of β can be written as $\beta = \beta_0 \exp(-E_E/kT)$, where E_E is the activation energy for detachment of atoms from island edges. Within the picture used here, E_E is equal to the sum of the activation barrier for terrace diffusion of adatoms (from D) and the difference in binding energy of an atom at the island edge (i.e., at a kink site) and on the terrace (from ρ_∞). Equation (3) describes exactly the decay of a circular adatom island placed concentrically within a circular vacancy island.

The extension of the theory to the decay of vacancy islands inside larger vacancy islands is straightforward. Whereas the flux of adatoms at the outer boundary and of diffusing adatoms between the step edges can still be described by Eqs. (1) and (2), respectively, the flux at the inner boundary of the vacancy island is changed by a factor $s = \nu_S/\nu_0 \exp(-E_S/kT)$, where E_S is the Ehrlich-Schwoebel barrier, and ν_S and ν_0 are the attempt frequencies for diffusion across the step and on the terrace, respectively. The diffusion constant D in Eq. (1) must be replaced by Ds, and, hence,

$$\frac{d(\pi r^2)}{dt} = \beta\left[\frac{a}{sr} + \ln(R/r) + \frac{a}{R}\right]^{-1} \times \left[\exp\left(-\frac{\gamma}{kTnr}\right) - \exp\left(-\frac{\gamma}{kTnR}\right)\right]. \tag{4}$$

Equations (3) and (4) can be solved by numerical integration. The resulting curves for the island area versus time can be fitted to the experimentally obtained curves by varying the parameters β, s, and γ. In general, very good fits are obtained as seen in Fig. 3.

Equation (3) shows that β essentially determines the time scale on which the decay proceeds, while γ influences the shape of the decay curves for small island sizes when the exponential functions cannot be approximated by a linear expansion [10]. The same holds for a given value of s in the case of vacancy islands [Eq. (4)]. The shape, however, is also affected by the slow temperature drift towards room temperature during measurements below or above room temperature. Therefore, we estimated γ from fits to the small-size part of decay curves taken at room temperature. The resulting value (from simultaneous fits to three adatom island and four vacancy island) is $\gamma = (0.75 \pm 0.15)$ eV/nm, where the error is obtained from a standard χ^2 analysis. This value is used as a fixed parameter in the analysis of decay curves above or below room temperature. Moreover, the analysis was limited to decay curves (or parts of decay curves) for which the temperature drift was less than 4 K. In Fig. 4, we show the β values and their errors obtained from fitting the adatom decay curves using standard least-squares minimization. An Arrhenius behavior of β over 3 orders of magnitude is found and the resulting activation energy for adatom detachment from the island edges is

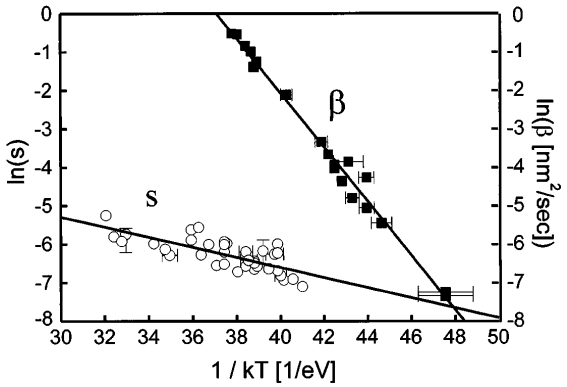

FIG. 4. Arrhenius plot for island decay: temperature dependence of β and s. Open circles: vacancy island decay; solid squares: adatom island decay; unless indicated, the error bars are smaller than the symbols.

$E_E = (0.71 \pm 0.03)$ eV. To check the stability of this analysis with respect to the choice of γ, we varied γ between 0.4 and 1 eV/nm and found that the change in E_E is within the error margins given. From the prefactor of β deduced from the Arrhenius plot, an attempt frequency for atom detachment of $\nu_0 = 10^{12\pm0.6}\ \mathrm{s}^{-1}$ is obtained.

With β determined from adatom island decay and choosing $\gamma = 0.75$ eV/nm, s can be determined from the vacancy island decay curves using Eq. (4) and a similar fitting procedure. Results at different temperatures are given in the Arrhenius plot in Fig. 4 from which the Ehrlich-Schwoebel barrier and the attempt frequency ratio are determined to $E_S = (0.13 \pm 0.04)$ eV and $\nu_S/\nu_0 = 10^{-0.6\pm0.5}$. In this case, a variation of γ hardly affects the result as s is essentially determined as the ratio of two quantities which shift by the same factor as γ is varied. Hence, the error given includes only the error of the linear fit in the Arrhenius plot and the uncertainty of β at fixed γ.

The latter result agrees well with previous estimates for the Ehrlich-Schwoebel barrier based on an analysis of nucleation kinetics on Ag(111) [(0.12 ± 0.02) eV [4], (0.15 ± 0.04) eV [5]]. Also, the value for the activation barrier for evaporation is reasonable. Using effective medium theory, Stoltze calculated an energy of formation of adatoms from kinks on Ag(111) of 0.555 eV and an adatom diffusion barrier of 0.064 eV [21,22]. The sum of the two energies corresponds to E_E and gives 0.62 eV. The agreement is even better (0.66 eV) if we use a diffusion barrier of 0.1 eV, as determined experimentally by Brune *et al.* [3]. The good agreement confirms the reliability of our approach. We are confident that the method presented in this paper can be used, in general, for determining energies that are crucial for crystal growth and surface dynamics on metal surfaces. The results can be used to understand more complicated processes like Ostwald ripening or the decomposition of multilayered nanostructures.

We acknowledge financial support from the Danish National Research Foundation through the Center for Atomic-scale Materials Physics (CAMP) and the Center for Nanotribology.

*Present address: Institute for Experimental Physics, University of Lausanne, 1015 Lausanne, Switzerland.
†Present address: Faculty of Applied Physics, University of Twente, 7500 AE Enschede, The Netherlands.
‡Present address: Institut für Physikalische und Theoretische Chemie, Universität Bonn, 53115 Bonn, Germany.

[1] For example, S. C. Wang and G. Ehrlich, J. Chem. Phys. **94**, 4071 (1991); G. Kellogg, Phys. Rev. Lett. **76**, 98 (1996).
[2] For recent reviews, see G. Kellogg, Surf. Sci. Rep. **21**, 1 (1994); G. Ehrlich, Surf. Sci. **299/300**, 628 (1994).
[3] H. Brune *et al.*, Phys. Rev. Lett. **73**, 1955 (1994); M. Bott *et al.*, Phys. Rev. Lett. **76**, 1304 (1996).
[4] K. Bromann *et al.*, Phys. Rev. Lett. **75**, 677 (1995).
[5] J. A. Meyer *et al.*, Phys. Rev. B **51**, 14 790 (1995).
[6] For example, A. Golzhäuser and G. Ehrlich, Phys. Rev. Lett. **77**, 1334 (1996); M. Poensgen *et al.*, Surf. Sci. **274**, 430 (1992); L. Kuipers, M. S. Hoogeman, and J. W. M. Frenken, Phys. Rev. Lett. **71**, 3517 (1993); for a review of FIM studies, see G. Ehrlich, Surf. Sci. **331–333**, 865 (1995).
[7] T.-Y. Fu, Y.-R. Tzeng, and T. T. Tsong, Phys. Rev. Lett. **76**, 2539 (1996).
[8] D. R. Peale and B. H. Cooper, J. Vac. Sci. Technol. A **10**, 2210 (1992).
[9] J.-M. Wen *et al.*, Phys. Rev. Lett. **76**, 652 (1996).
[10] K. Morgenstern, G. Rosenfeld, and G. Comsa, Phys. Rev. Lett. **76**, 2113 (1996).
[11] S. C. Wang and G. Ehrlich, Surf. Sci. **239**, 301 (1990).
[12] J. P. Barbour *et al.*, Phys. Rev. **117**, 1452 (1960).
[13] G. Ehrlich and F. G. Hudda, J. Chem. Phys. **44**, 1039 (1966); R. L. Schwoebel and E. J. Shipsey, J. Appl. Phys. **37**, 3682 (1966).
[14] B. K. Chakraverty, J. Phys. Chem. Solids **28**, 2401 (1967).
[15] P. Wynblatt and N. A. Gjostein, in *Progress in Solid State Chemistry,* edited by J. O. McCardin and G. Somorjai (Pergamon, Oxford, 1975),Vol. 9, pp. 21.
[16] M. Zinke-Allmang, L. C. Feldman, and M. H. Grabow, Surf. Sci. Rep. **16**, 377 (1992).
[17] J. G. McLean *et al.*, Phys. Rev. B **55**, 1811 (1997).
[18] A. Ichimiya, T. Tanaka, and K. Ishiyama, Phys. Rev. Lett. **76**, 4721 (1996).
[19] L. Eierdal *et al.*, Surf. Sci. **312**, 31 (1994).
[20] K. Morgenstern, G. Rosenfeld, and G. Comsa, Surf. Sci. **352–354**, 956 (1996).
[21] P. Stoltze, J. Phys. Condens. Matter **6**, 9495 (1994).
[22] Similar values are obtained by the Embedded Atom Method: R. C. Nelson *et al.*, Surf. Sci. **295**, 462 (1993).